OBSERVATIONS OF THE ROTATIONAL TRANSITIONS OF OH FROM THE ORION MOLECULAR CLOUD

GRANT NAG2 – 311

Semiannual Report Nos. 6, 7, 8, and 9
For the period 1 April 1987 to 31 March 1989

Principal Investigator
Dr. Gary J. Melnick

March 1989

Prepared for the
National Aeronautics and Space Administration
Ames Research Center
Moffett Field, California 94035

Smithsonian Institution
Astrophysical Observatory
Cambridge, Massachusetts 02138

The Smithsonian Astrophysical Observatory
is a member of the
Harvard-Smithsonian Center for Astrophysics

Technical monitor for this grant is Mr. Louis C. Haughney, Medium Altitude Missions Branch, Code 211 – 12, NASA Ames.

The study of rotationally excited, far-infrared OH line emission from Orion-KL using the KAO has been highly productive. The Table below summarizes the flight series and their accomplishments since December 1984.

Summary of Observations

Date of Observations	In Collaboration with ...	OH Line Observed
December 1984	Houck Cornell University	46.19 μm $^2\Pi_{1/2}$ $J = 11/2 \rightarrow 9/2$
February 1985	Townes, Genzel U. C. Berkeley	163.2 μm $^2\Pi_{1/2}$ $J = 3/2 \rightarrow 1/2$ 162.8 μm CO $J = 16 \rightarrow 15$
February 1986	Houck Cornell University	46.19 μm $^2\Pi_{1/2}$ $J = 11/2 \rightarrow 9/2$ 34.61 μm $^2\Pi_{1/2}$ $J = 5/2 \rightarrow {}^2\Pi_{3/2}$ $J = 3/2$
January 1987	Townes, Genzel U. C. Berkeley	119.2 μm $^2\Pi_{3/2}$ $J = 5/2 \rightarrow 3/2$ 53.35 μm $^2\Pi_{1/2}$ $J = 3/2 \rightarrow {}^2\Pi_{3/2}$ $J = 3/2$ 120.2 μm ^{18}OH $^2\Pi_{3/2}$ $J = 5/2 \rightarrow 3/2$

To date, the publications that have resulted from these observations are:

1. Observations of Rotational Transitions of OH from OMC-1, Gary Melnick, in *Masers, Molecules, and Mass Outflows in Star Forming Regions*, A.D. Haschick (ed.), Haystack Observatory Press, p. 33 (1986).

2. Observations of Far-Infrared Line Profiles in the Orion-KL Region, Michael K. Crawford, John B. Lugten, W. Fitelson, Reinhard Genzel, and Gary Melnick, *Ap. J.*, **303**, L57 (1986).

5. "Infrared Line Emission from High Velocity Outflows in Star Forming Regions." Invited review talk given at the 22nd European Space Agency Symposium on Infrared Spectroscopy in Astronomy, Salamanca, Spain, December 7 – 9, 1988.

In addition, a paper analyzing the results of the January 1987 flight series is about to be submitted. A copy of this paper is attached.

FURTHER OBSERVATIONS OF ROTATIONALLY EXCITED FAR-INFRARED ^{16}OH AND ^{18}OH EMISSION IN ORION-KL: TIGHTER CONSTRAINTS ON THE NATURE OF THE EMITTING REGION

G. J. Melnick
Harvard-Smithsonian Center for Astrophysics

R. Genzel, A. Poglitsch
Max-Planck Institut für Physik und Astrophysik
Institut für extraterrestrische Physik, Garching, FRG

G. J. Stacey and J. B. Lugten
Department of Physics, University of California, Berkeley

ABSTRACT

We have observed the region within 1 arc-minute of Orion-KL and report the first detections of the ^{16}OH $^2\Pi_{1/2} \rightarrow {}^2\Pi_{3/2}$ $J = 3/2^- \rightarrow 3/2^+$ rotational cross-ladder transition (53.351 μm) and the ^{18}OH $^2\Pi_{3/2}$ $J = 5/2^+ \rightarrow 3/2^-$ rotational ground-state transition (120.1719 μm). We find that both of these lines exhibit a P-Cygni profile. In addition, we have velocity resolved the ^{16}OH $^2\Pi_{3/2}$ $J = 5/2^- \rightarrow 3/2^+$ rotational ground-state transition (119.234 μm) and find that its intrinsic full-width at half-maximum is 25 km s^{-1}. We model both the line fluxes and line profiles, along with the previously measured ^{16}OH $^2\Pi_{3/2}$ 84 μm and $^2\Pi_{1/2}$ 163 μm rotational transitions, and find that no single temperature and density component can reproduce the data. Rather, the best overall fit to the data requires emission from three main components of the gas: (1) post-shocked gas with the profiles of temperature, density, and

OH abundance like that predicted by Draine and Roberge (1982) for a 38 km s^{-1} C-type shock, (2) a higher density ($H_2 \simeq 2 \times 10^7$ cm^{-3}) component to the cool post-shocked region than given by Draine and Roberge, and (3) the plateau region. All three components require a significant radiative background in order to fit the data.

Subject Headings: infrared spectra - interstellar molecules: nebulae: Orion Nebula

I. INTRODUCTION

^{16}OH far-infrared line emission from excited rotational states was first detected toward the embedded star-forming region in Orion-KL by Storey *et al.* (1981). Though the OH line widths were unresolved in these early measurements, two observational features lead these authors to assume that the OH $^2\Pi_{3/2}$ $J = 5/2 \rightarrow 3/2$ 119 μm emission they detected comes from the shocked gas region surrounding BN-KL: (1) the emitting region had to be warm since the OH lines were seen in emission and the temperatures above the ground state for the upper $J = 5/2$ levels are $\simeq$ 121 K and, (2) the OH emission was observed 30″ north of KL, toward the peak of the shock-excited H_2 emission (e.g., Beckwith *et al.* 1978). Subsequent observations, with improved spectrometer sensitivity and spectral resolution, have resulted in the detection of two additional far-infrared, rotational doublet transitions: the $^2\Pi_{3/2}$ $J = 7/2 \rightarrow 5/2$ lines at 84.4202 and 84.5966 μm and the $^2\Pi_{1/2}$ $J = 3/2 \rightarrow 1/2$ lines at 163.121 and 163.396 μm (Watson *et al.* 1985; Viscuso *et al.* 1985; Viscuso *et al.* 1985*a*; Melnick *et al.* 1987). Unfortunately, even with the detection of six OH far-infrared rotational transitions, it was not possible to distinguish between a variety of different models for the emitting region, including shocks and a number of non-shock scenarios (see Melnick *et al.* 1987, hereafter referred to as Paper I, for a review of these models).

In this paper, we present the first observations of two additional OH far-infrared transitions, the ^{16}OH $^2\Pi_{1/2} \rightarrow {}^2\Pi_{3/2}$ $J = 3/2^- \rightarrow 3/2^+$ cross-ladder transition at 53.351 μm (see Figure 1) and the ^{18}OH $^2\Pi_{3/2}$ $J = 5/2^+ \rightarrow 3/2^-$ rotational ground-state transition at 120.1719 μm, plus a spectrum of the previously observed ^{16}OH $^2\Pi_{3/2}$ $J = 5/2^- \rightarrow 3/2^+$ 119.234 μm line which has now been velocity resolved. Because the intensities *and profiles* of these lines are sensitive to the radiative background, density, temperature, and gas velocity, these transitions can now be used to considerably narrow the range of conditions in the OH emitting region. Here we present a model of the OH emitting regions which successfully accounts for the observed line emission.

II. Observations and Results

The observations were carried out 1986 November and 1987 January using the 91 cm telescope aboard the Kuiper Airborne Observatory. The data were taken with the Mk II UCB cryogenic tandem Fabry-Perot spectrometer (Lugten 1987). The spectra were obtained with the beam centered on the Becklin-Neugebauer object ($\alpha_{1950} = 5^h\,32^m\,47^s$, $\delta_{1950} = 5^\circ\,24'\,17''$). The ^{16}OH $^2\Pi_{3/2}$ $J = 5/2^- \rightarrow 3/2^+$ 119.234μm spectra were taken at resolutions (FWHM) of 40 and 24 km s^{-1}, while the ^{16}OH $^2\Pi_{1/2} \rightarrow {}^2\Pi_{3/2}$ $J = 3/2^- \rightarrow 3/2^+$ transition at 53.351 μm and the ^{18}OH $^2\Pi_{3/2}$ $J = 5/2^+ \rightarrow 3/2^-$ line at 120.1719 μm were observed with spectral resolutions of 38 and 55 km s^{-1}, respectively. Due to terrestrial O_3 and H_2O absorption, neither the accompanying ^{16}OH $^2\Pi_{1/2} \rightarrow {}^2\Pi_{3/2}$ $J = 3/2^+ \rightarrow 3/2^-$ 53.261 μm or ^{18}OH $J = 5/2^- \rightarrow 3/2^+$ 119.9659 μm transitions were observed.

The telescope's secondary was chopped at a frequency of 33 Hz with an amplitude of 3.'7 in azimuth (approximately east-west). The line fluxes were derived from the measured line-to-continuum ratio and the photometric measurements of Orion-KL (M. Werner, private communication). Table 1 summarizes our results

along with selected previous observations of OH from Orion-KL (a more complete listing of previous OH rotational data is provided in Paper I). The spectra of the individual OH lines are shown in Figures 2 – 4. The uncertainty in the absolute value of the continuum is the largest source of error and limits the accuracy of the derived fluxes to approximately 30%. The absolute velocity (and wavelength) scale was determined relative to H_2S (53.3242 μm), $HD^{18}O$ (119.3950 μm), and D_2O (120.2554 μm) absorption in a gas cell and is accurate to $\pm$ 3 km s^{-1}.

The three main results of our most recent observations are:

(1) We have detected the first isotopic counterpart of a far-infrared rotational line. The ^{18}OH 120.1719 μm line, counterpart of the ^{16}OH 119.441 μm transition, is observed in absorption in the velocity range between approximately -100 and $+10$ km s^{-1} and in emission between about $+10$ and $+80$ km s^{-1}.

(2) We report the first detection of an OH cross-ladder transition. The ^{16}OH 53.351 μm line is observed strongly in absorption in the velocity range between -100 and $+10$ km s^{-1} and more weakly in emission between $+10$ and $+80$ km s^{-1}.

(3) The previously observed ^{16}OH 119.234 μm transition was re-observed with sufficient spectral resolution, 24 km s^{-1}, to determine that its FWHM is 25 km s^{-1}. This compares with a FWHM for the 163.121 μm line of $\simeq$ 45 km s^{-1} (Crawford *et al.* 1986). The peak of the 119.234 μm line emission occurs at a $v_{\rm LSR}$ of $+10$ km s^{-1}.

A number of general conclusions emerge from the data, independent of the model adopted:

(1) Assuming that the ^{18}OH 120 μm transition is optically thin and that the ^{16}OH : ^{18}OH abundance ratio is 500 : 1 (cf., Comben *et al.* 1986), then, by assuming LTE, the *minimum* ^{16}OH column density responsible for the far-infrared emission we detect is determined to be 3×10^{15} cm^{-2}.

(2) The relative strengths of the ^{16}OH 53.351 μm absorption feature and the

163.396 μm emission line previously detected (e.g., Melnick *et al.* 1987) clearly demonstrate the importance of radiative excitations. In fact, a comparison of the excitation rate to the $^2\Pi_{1/2}$ $J = 3/2^-$ level due to the absorption of 53.351 μm photons, 8×10^3 photons cm^{-2} s^{-1} ($\Leftrightarrow$ 3×10^{-10} erg cm^{-1} s^{-1}), with the de-excitation rate out of that level via 163.396 μm photons, 1×10^4 photons cm^{-2} s^{-1} ($\Leftrightarrow$ 1.3×10^{-10} erg cm^{-1} s^{-1}), shows that radiation dominates collisions in exciting the $^2\Pi_{1/2}$ $J = 3/2$ levels.

(3) As noted in Melnick *et al.* (1987), the comparable strengths of the 84 and 119 μm lines require that a significant portion of the OH emitting region has temperatures greater than 50 K, densities greater than 10^7 cm^{-3}, or both.

(4) The symmetry of the ^{18}OH 120 μm P-Cygni profile indicates that most of the OH emitting gas is involved in radial expansion from BN-KL with a maximum velocity difference between the emitting and absorbing gas of 80$-$100 km s^{-1}.

III. CALCULATIONS

In order to model the ^{16}OH line intensities, the equations of statistical equilibrium and line formation for the lowest 30 levels of the OH molecule have been solved; these include all levels up to the $J = 17/2$ level in the $^2\Pi_{3/2}$ ladder and the $J = 13/2$ level in the $^2\Pi_{1/2}$ ladder. These calculations take account of the Λ-doubling, but ignore the hyperfine structure. The radiative transition probabilities were provided by Black and van Dishoeck (1985, private communication) based on the transition matrix elements computed by van Dishoeck (1984). Dewangan *et al.* (1987) have calculated the OH-H_2 excitation rate coefficients for the lowest 18 rotational transitions. Downward transition rates are obtained using the principle of detailed balance. Additional rate coefficients were obtained from Lülf (1985), Schinke and Andresen (1984), and van Dishoeck (1985, private communication). In all cases, the downward rate coefficients are taken to be independent of tempera-

ture. For lack of any published rate coefficients for ^{18}OH, the rate coefficients for ^{16}OH were assumed to apply.

As discussed in section II, radiative processes must be considered along with collisional processes. For Orion-KL, the intensity of the local radiation field is represented by an infrared continuum of the form

$$I_\nu^C = B_\nu(T_c)\left\{\tau_o \times \left[\frac{60}{\lambda(\mu\mathrm{m})}\right]\right\} \quad (1)$$

where B_ν = Planck function at the color temperature of the continuum, T_c. Taking T_c = 72 K and τ_o = 0.503 reproduces the 20-100 μm flux density of Orion-KL measured with a 50″ beam by Erickson *et al.* (1981) and is consistent with the 400 μm flux density measured with 35 and 90″ beam sizes by Keene *et al.* (1982).

A twofold approach was taken to modelling the OH emitting gas: (1) an attempt was made to fit the data with one gas component, characterized by a single temperature, density, OH abundance, velocity gradient, and radiation background, and (2) a sum was made of the contributions from several known components, such as the shocked gas, plateau, compact ridge, and hot core regions. Conditions characterizing the plateau, compact ridge, and hot core regions have been determined through studies of a variety of molecules and are summarized by a number of authors (e.g., Wynn-Williams *et al.* 1984; Masson *et al.* 1984; Blake *et al.* 1987). Less is known of the conditions that prevail in the shocked gas region where the observed outflowing gas impacts the surrounding quiescent material. In general, the models which come closest to reproducing the existing high-J CO, fine-structure [OI], and ro-vibrational H_2 lines invoke the presence of a magnetohydrodynamic "C-type" shock (cf., Draine and Roberge 1982; Chernoff *et al.* 1982). Though more recent CO and H_2 data have highlighted shortcomings in these C-type models, we use the profiles of temperature, density, velocity, and OH abundance given by Draine and Roberge (1982) as the basis for our shock calculations. Discrepancies between this

assumed shock model and the OH data will be discussed in section V.

The geometry of each component is idealized as spherical, except for the shocked gas region which was assumed to be a thin, spherical shell. In all cases the gas was assumed to be symmetrically distributed around the central continuum source. Because the measured velocity widths of the OH lines are between 25 and 50 km s^{-1} (Crawford *et al.* 1986; this work), the radiative transfer in the lines was solved simultaneously with the level populations under the large velocity gradient approximation (Sobolev 1960). In addition to the line intensities, the intrinsic line profiles were calculated from each component. In order to relate these profiles to those observed, the intrinsic line profiles were convolved with a Lorentzian profile with a FWHM equal to the instrumental spectral resolution achieved for each line.

IV. Results of Modelling

In Paper I, fits to the then available 84, 119, and 163 μm line data were obtained with a number of different single-component models. A re-examination of these models in light of the most recent data indicates that all fail to reproduce the strong 53 μm absorption observed; at the densities suggested for most of those models, i.e., $n_{H_2} > 5 \times 10^7$ cm^{-3}, the profile of the 53 μm line would be mostly in emission and only weakly in absorption. Even our best single component fit ($T_c = 150$ K, $T_{gas} = 80$ K, $n_{H_2} = 4 \times 10^6$ cm^{-3}, and $dv/dr = 500$ km s^{-1} pc^{-1}) results in a 53 μm profile which exhibits almost equal emission and absorption, contrary to what is observed. Attempts to fit the 53 μm line profile by lowering the gas temperature has the effect of reducing the expected 84 μm line flux below its detected value. We therefore conclude that *no* single temperature, density, and velocity gradient model adequately reproduces the measured line fluxes and profiles.

Instead, the best fit to the data is obtained by assuming emission from three main regions; (1) the *C*-type shocked gas region, (2) a dense ($n_{H_2} \simeq 2 \times 10^7$ cm^{-3}),

warm ($T \simeq 75$ K) addition to the post-shocked region, and (3) the high velocity plateau. The two post-shocked components are thin (few $\times 10^{15}$ cm), but are assumed to subtend about $43''$ – corresponding roughly to the observed separation in both the [OI] 63μm and H_2 $v = 1 \rightarrow 0$ $S(1)$ 2.12μm emission peaks (Werner *et al.* 1984; Beckwith *et al.* 1978). The high velocity plateau is assumed to encompass the $\Delta v \geq 18$ km s^{-1} gas observed within about $20''$ of IRc 2. A summary of these best fit conditions is given in Table 2.

A comparison of the observed line fluxes and those predicted by this model is shown in Figure 5. The computed line profiles for each contributing component along with the resulting combined profile are shown in Figures 6 – 9. As is clear from these figures, most of the OH emission we observe arises in the shocked gas region. While agreement with the measured line fluxes could be obtained with only the shocked gas region simply by assuming a somewhat larger shock diameter, the resulting line profiles are at greater variance with the observations than emission from several components. In particular, for expected continuum backgrounds, emission from the shocked gas component alone results both in a slight P-Cygni profile for the ^{16}OH 119.234 μm line and a narrower ^{16}OH 163.121 μm line than is observed. The presence of a higher density region within the post-shocked gas is suggested mostly by its effect on the line profiles; such a component, sharing in the 38 km s^{-1} velocity of the shock, serves to broaden all of the OH lines we observe. Supporting evidence for higher densities in the post-shocked region, beyond the OH data presented here, is discussed in the next section.

It is interesting to note that the ^{18}OH 120 μm and, to a lesser extent, the ^{16}OH 53 μm P-Cygni profiles indicate that there is no significant OH rotational emission from regions having both a $v_{\rm LSR}$ near $+9$ km s^{-1} and small internal gas velocities (< 10 km s^{-1}). OH line emission from such regions at levels greater than about 10 percent of the total measured 120 μm and 53 μm line fluxes would begin to distort these line profiles in ways which are not seen. Thus, it is inferred that the

hot core, compact ridge, and extended ridge are not major sources of OH rotational line radiation.

IV. DISCUSSION

In this section we shall discuss the plausibility of our 3-component model for the OH emission. Specifically, we review the reasons why the shocked gas region, the high density post-shock gas, and the plateau are reasonable OH sources, while the hot core and compact ridge may be less likely candidates for the OH emission we detect.

(a) Post-Shocked Gas

The relatively fast moving ($v_s \sim 40$ km s^{-1}) shock surrounding IRc 2/BN-KL provides a natural explanation for both the broad profiles observed in the 119 and 163 μm lines and the P-Cygni profiles seen in the 53 μm and ^{18}OH 120 μm transitions. Beyond this phenomenological association with the shocked gas region, the predicted abundance of OH within the post-shock zone is sufficiently high that, under the prevailing density and temperature conditions, strong OH emission is *expected* from this gas.

Behind a *C*-type shock such as we consider here, the gas temperatures drop from a peak of about 3000 K to 50 K over a distance of $\sim 2 - 3 \times 10^{15}$ cm. Under these conditions, the gas phase abundance of OH is governed by relatively few reactions, the two most important being:

$$O + H_2 \rightarrow OH + H$$
$$OH + H_2 \rightarrow H_2O + H\,.$$

These reactions are endothermic, possessing activation energies of a few hundred degrees, but proceed rapidly once the thermal energy of the gas is sufficiently warm.

For the profiles of temperature and density given by Draine and Roberge (1982) the above reactions yield an abundance of OH within the post-shocked gas, f(OH) ($\equiv [N(\mathrm{OH})/N(\mathrm{H_2})]$), of between 2×10^{-5} and 4×10^{-7}. For a reasonable value of the shock radius, 43″, and radiative background, $T_c = 80\,\mathrm{K}$, the range of gas densities, temperatures, velocity gradients, and OH abundances given by the Draine and Roberge model (1982) comes close to accounting for the OH emission we observe.

(b) High Density Post-Shocked Zone

A better fit to line profiles is obtained by assuming that the shock model described by Draine and Roberge possesses higher density gas in the post-shocked zone than is assumed in their model. Supportive evidence for higher densities in the post-shock flow is provided by recent observations of vibration-rotation and pure rotation lines of H_2 as well as CO vibration-rotation band emission toward H_2 Peak 1.

Recently, Brand *et al.* (1988) have reviewed the column densities needed to achieve the measured intensities of a total of 19 previously and newly detected H_2 lines from the shocked gas region in Orion-KL (H_2 Peak 1). Of particular interest here is their finding that the *C*-type shocks proposed by Draine and Roberge (1982) and Chernoff *et al.* (1982) underestimate the column densities needed to explain the H_2 data at both high temperatures ($T_{\mathrm{gas}} \geq 3 \times 10^3\,\mathrm{K}$) and low temperatures ($T_{\mathrm{gas}} \leq 1000\,\mathrm{K}$) by about a factor of 10. At the higher temperatures this finding has little effect on the predicted OH line flux since the total column density of this hot gas is low. However, at the lower temperatures, the higher column densities are reflected in the line fluxes and profiles.

Similarly, the detection of the 4.7 μm fundamental vibration-rotation band of CO in emission toward H_2 Peak 1 (Geballe and Garden 1987) requires densities and column densities in excess of that predicted by the *C*-type shock models. Specifically, a density of $10^7\ \mathrm{cm^{-3}}$ and a column density of $2 \times 10^{22}\ \mathrm{cm^{-2}}$ are necessary to excite the 4.7 μm fundamental vibration-rotation band into emission.

(c) Plateau, Hot Core, and Compact Ridge

Like the shocked gas region, OH emission from the high velocity gas in the plateau fits the observed line profiles. However, significant OH emission from the low velocity gas within the hot core and compact ridge is not consistent with the measured ^{18}OH 120 μm P-Cygni profile. This distinction between regions likely results from a larger OH abundance in the plateau than either the hot core or compact ridge.

Within the warm gas found in the plateau, hot core, and compact ridge, OH can be formed in two ways. First, recombination of H_3O^+ can produce both H_2O and OH via the reaction

$$H_3O^+ + e^- \rightarrow H_2O + H$$

$$\rightarrow OH + H_2 \ .$$

Second, even when H_2O is preferentially produced via the above reaction, the OH abundance subsequently can be increased by the photodissociation of water,

$$H_2O + h\nu \rightarrow OH + H \, ,$$

where the cross-section for photodissociation is highest for photon wavelengths between 1000 and 1800 Å. For the conditions within the plateau, hot core, and compact ridge, these processes lead to an f(OH) between 10^{-11} and 10^{-8} (Lepp, private communication), too low to result in significant far-infrared OH emission. However, recent interferometric observations of HDO in Orion-KL by Plambeck and Wright (1987) indicate an unexpectedly high HDO/H_2 abundance of $\sim 10^{-7}$ toward both the hot core and compact ridge which, like the anomalously high abundance of NH_3, HCN, CH_3OH, and NH_2D in these regions, is believed to be due to the evaporation of these species from dust grain mantles. H_2O released in this manner would be quickly converted to OH via photodissociation in those regions exposed to a strong

ultraviolet (UV) field. That HDO is predominantly observed in the hot core and compact ridge, with only a small contribution from the plateau, suggests that self-shielding against UV photodissociation is less effective in the high velocity gas. This would lead to a higher OH abundance in the plateau than either the hot core or compact ridge, which is consistent with our model. Significant OH emission from the extended ridge is not expected due to the low density ($\sim 10^5$ cm^{-3}) and low temperature ($\sim$ 50 K) of this region.

V. SUMMARY

We report the first detection of two important OH far-infrared, rotational transitions: (1) the ^{16}OH $^2\Pi_{1/2} \rightarrow {}^2\Pi_{3/2}$ $J = 3/2^- \rightarrow 3/2^+$ cross-ladder transition at 53.351 μm and the ^{18}OH $^2\Pi_{3/2}$ $J = 5/2^+ \rightarrow 3/2^-$ rotational ground-state transition at 120.1719 μm. This data, along with previously obtained OH rotational line data, show the following:

(1) The minimum ^{16}OH column density toward Orion-KL is 3×10^{15} cm^{-2}.

(2) Radiative excitations play an important role in populating the rotational energy levels of OH in Orion-KL, as evidenced by the ratio of the ^{16}OH 53.351 μm absorption and 163.396 μm emission intensities.

(3) The width of the ^{16}OH 119 and 163 μm lines along with the P-Cygni profiles exhibited by the ^{16}OH 53 μm and ^{18}OH 120 μm lines confirms that the origin of most of the OH emission we detect is associated with high velocity gas.

(4) No single component model can account for the observed OH line fluxes and profiles.

(5) The best fit to the data assumes that the OH emission arises within a *C*-type shock of the type described by Draine and Roberge (1982) and Chernoff *et al.* (1982) with a higher density post-shocked region than given in these models. Emission from the plateau source also contributes to the OH flux we detect. All

regions are subject to a strong infrared continuum background.

(6) The hot core, compact ridge, and extended ridge do not contribute significantly to the detected OH emission.

ACKNOWLEDGEMENTS

We thank the staff of the Kuiper Airborne Observatory for their support. We also wish to acknowledge helpful discussions with S. Lepp and C. Masson. This work was supported by NASA grant NAG 2-311.

TABLE 1.

SUMMARY OF OH ROTATIONAL DATA USED TO MODEL EMITTING REGION IN ORION-KL

Line	λ (μm)	FWHM Beam Size	Flux in Emission [a] (10^{-17} W cm^{-2})	Flux in Absorption [a] (10^{-17} W cm^{-2})	Intensity in Emission [a,b] (10^{-3} erg s^{-1} cm^{-2} sr^{-1})	Intensity in Absorption [a,b] (10^{-3} erg s^{-1} cm^{-2} sr^{-1})
^{16}OH						
$^2\Pi_{3/2}$ $J = 7/2^- \rightarrow 5/2^+$	84.5966	1′	1.4 ± 0.4 [c]	—	1.4	—
$^2\Pi_{1/2}$ $J = 3/2^+ \rightarrow 1/2^-$	163.121	55″	1.3 [d,e]	—	1.6	—
$^2\Pi_{3/2}$ $J = 5/2^- \rightarrow 3/2^+$	119.234	45″	1.88 [f,g]	—	3.3	—
$^2\Pi_{1/2}$ $J = 3/2^- \rightarrow {}^2\Pi_{3/2}$ $J = 3/2^+$	53.3512	40″	0.63 [f,h]	3.0 [f,h]	1.4	6.6
^{18}OH						
$^2\Pi_{3/2}$ $J = 5/2^+ \rightarrow 3/2^-$	120.1719	45″	0.03 [f,i]	0.06 [f,i]	0.05	0.11

[a] Uncertainty in the absolute fluxes and intensities is ± 30% unless indicated otherwise.

[b] Solid angles for different beam sizes are 8×10^{-8} sr for 55″ beam, 5.7×10^{-8} sr for 45″, and 4.5×10^{-8} sr for 40″.

[c] Viscuso *et al.* (1985).

[d] Melnick, Genzel, and Lugten (1987).

[e] Velocity resolution = 60 km s^{-1}.

[f] This work.

[g] Velocity resolution = 24 km s^{-1}.

[h] Velocity resolution = 38 km s^{-1}.

[i] Velocity resolution = 55 km s^{-1}.

TABLE 2.

BEST-FIT MODEL OF OH EMISSION IN ORION-KL

Component	v_{LSR} (km s^{-1})	Δv (km s^{-1})	T_{gas} (K)	T_c (K)	n_{H_2} (cm^{-3})	OH/H_2	θ_{source}[a] (arc-seconds)	N_{H_2} (cm^{-2})
Plateau	7	30	95	130	2×10^6	2×10^{-7}	20	3×10^{23}
Shock[b]	7	38	2700 – 30	80	4×10^5 – 7×10^6	2×10^{-5} – 4×10^{-7}	43	3×10^{21} [c]
High Density Post-Shock[d]	7	6	75	80	2×10^7	4×10^{-7}	43	2×10^{22} [c]

[a] Assumes that the OH emission fills the area within θ_{source}.

[b] Calculation of the OH emission from the shocked gas region is based on the profiles of temperature, density, and abundance given by Draine and Roberge (1982).

[c] Normal to a single shock surface; assumes that all of the hydrogen is in the form of H_2.

[d] See text.

REFERENCES

Beckwith, S., Persson, S.E., Neugebauer, G., and Becklin, E.E. 1978, *Ap. J.*, **223**, 464.

Blake, G.A., Sutton, E.C., Masson, C.R., and Phillips, T.G. 1987, *Ap. J.*, **315**, 621.

Brand, P.W.J.L., Moorhouse, A., Burton, M.G., Geballe, T.R., Bird, M., and Wade, R. 1988, *Ap. J. (Letters)*, **334**, L103.

Chernoff, D.F., Hollenbach, D.J., and McKee, C.F. 1982, *Ap. J. (Letters)*, **259**, L97.

Comben, E.R., Brown, J.M., Steimle, T.C., Leopold, K.R., and Evenson, K.M. 1986, *Ap. J.*, **305**, 513.

Crawford, M.K., Lugten, J.B., Fitelson, W., Genzel, R., and Melnick, G.J. 1986, *Ap. J. (Letters)*, **303**, L57.

Dewangan, D.P., Flower, D.R., and Alexander, M.H. 1987, *M.N.R.A.S.*, **226**, 505.

Draine, B.T., and Roberge, W.G. 1982, *Ap. J. (Letters)*, **259**, L91.

Erickson, E. F., Knacke, R. F., Tokunaga, A. T., and Haas, M. R. 1981, *Ap. J.*, **245**, 148.

Geballe, T.R., and Garden, R. 1987, *Ap. J. (Letters)*, **317**, L107.

Keene, J., Hildebrand, R. H., and Whitcomb, S. E. 1982, *Ap. J. (Letters)*, **252**, L11.

Lugten, J.B. 1987, Ph.D. thesis, University of California, Berkeley.

Lülf, H. W. 1985, private communication.

Masson, C.R., Berge, G.L., Claussen, M.J., Heiligman, G.M., Leighton, R.B., Lo, K.Y., Moffet, A.T., Phillips, T.G., Sargent, A.I., Scott, S.L., Wannier, P.G., and Woody, D.P. 1984, *Ap. J. (Letters)*, **283**, L37.

Melnick, G.J., Genzel, R., and Lugten, J.B. 1987, *Ap. J.*, **321**, 530.

Plambeck, R.L., and Wright, M.C.H. 1987, *Ap. J. (Letters)*, **317**, L101.

Schinke, R., and Andresen, P. 1984, *J. Chem. Phys.*, **81**, 5644.

Sobolev, V. V. 1960, *Moving Envelopes of Stars* (Cambridge: Harvard University Press).

Storey, J.W.V., Watson, D.M., and Townes, C.H. 1981, *Ap. J. (Letters)*, **244**, L27.

van Dishoeck, E. F. 1984, Ph. D. Thesis, University of Leiden.

Viscuso, P. J., Stacey, G. J., Fuller, C. E., Kurtz, N. T., and Harwit, M. 1985, *Ap. J.*, **296**, 142.

Viscuso, P. J., Stacey, G. J., Harwit, M., Haas, M. R., Erickson, E. F., and Duffy, P. B. 1985*a*, *Ap. J.*, **296**, 149.

Watson, D. M., Genzel, R., Townes, C. H., and Storey, J. W. V. 1985, *Ap. J.*, **298**, 316.

Werner, M.W., Crawford, M.K., Genzel, R., Hollenbach, D.J., Townes, C.H., and Watson, D.M. 1984, *Ap. J. (Letters)*, **282**, L81.

Wynn-Williams, C.G., Genzel, R., Becklin, E.E., and Downes, D. 1984, *Ap. J.*, **281**, 172.

FIGURE CAPTIONS

Figure 1. Part of the rotational energy level diagram of OH. The rotational ladder has two branches, $^2\Pi_{3/2}$ and $^2\Pi_{1/2}$, due to spin splitting. The Λ – doubling, which splits each rotational level into two sublevels, is not drawn to scale (the hyperfine splitting that gives rise to the maser transitions is not shown). Both the level J-value (J) and parity (p) are also indicated. The transitions of interest here are marked with solid lines along with the wavelength in microns.

Figure 2. Spectrum of the 53.351 μm ^{16}OH $^2\Pi_{1/2} \rightarrow {}^2\Pi_{3/2}$ $J = 3/2^- \rightarrow 3/2^+$ cross-ladder transition. The accompanying cross-ladder doublet transition at 53.261 μm was not observed due to interference from a terrestrial H_2O absorption feature at 53.2605 μm.

Figure 3. Spectrum of the 119.234 μm ^{16}OH $^2\Pi_{3/2}$ $J = 5/2^- \rightarrow 3/2^+$ transition.

Figure 4. Spectrum of the 120.1719 μm ^{18}OH $^2\Pi_{3/2}$ $J = 5/2^+ \rightarrow 3/2^-$ rotational ground-state transition. The accompanying ^{18}OH doublet transition at 119.9659 μm was not observed due to interference from a nearby terrestrial O_3 absorption feature at 119.9947 μm.

Figure 5. Comparison of model OH line fluxes with that observed. The model assumes OH far-infrared rotational line emission from three sources within the Orion-KL region: (1) a 43″ diameter, 38 km s^{-1} C-type shock like that described by Draine and Roberge (1982) and Chernoff *et al.* (1982), (2) a high density ($H_2 \simeq 2 \times 10^7$ cm^{-3}), warm ($T_{\rm gas} \simeq 75$ K) zone within the post-shock flow and, (3) the 20″ diameter plateau region. The plateau region is assumed to be subject to an infrared continuum background with $T_c = 130$ K, while the shock plus high density shell which are further from IRc 2 are assumed to see a central infrared continuum with

T_c = 80 K (see eqn. 1). A more complete listing of the best-fit conditions is given in Table 2. The observed OH line fluxes are indicated by the open boxes and the error bars reflect the ± 30 percent uncertainty in each value. The fluxes predicted by the model are shown as dark circles. The ^{16}OH 53 μm and ^{18}OH 120 μm lines, both of which exhibit a P-Cygni profile, are represented by two points each: one for the absorption line flux and the second for the emission line flux.

Figure 6. OH line profiles resulting from best-fit three-component model described in the text. In order to match the observed profiles, the predicted profiles were convolved with a Lorentzian line shape that has a full-width at half-maximum equal to the instrumental spectral resolution obtained for each line: 38 km s^{-1} at 53 μm, 40 km s^{-1} at 119 μm, 15 km s^{-1} at 163 μm, and 55 km s^{-1} for the ^{18}OH line at 120 μm. The 163 μm observations were obtained previously (Crawford *et al.* 1986). The peaks of the predicted line profiles have been normalized to the data.

Figure 7. Same as Figure 6, except for the contribution from the *C*-type shock alone. The intensity scale is the same as that used in Figure 6, thus permitting a direct assessment of the relative contribution from the shocked gas region to the final line profile.

Figure 8. Same as Figure 6, except for the contribution from the high density shell alone. The intensity scale is the same as that used in Figure 6, thus permitting a direct assessment of the relative contribution from the high density shell to the final line profile.

Figure 9. Same as Figure 6, except for the contribution from the plateau alone. The intensity scale is the same as that used in Figure 6, thus permitting a direct assessment of the relative contribution from the plateau to the final line profile.

Authors' addresses:

G. J. Melnick
Center for Astrophysics
60 Garden Street
Cambridge, MA 02138

R. Genzel and A. Poglitsch
Max-Planck Institut für Physik und Astrophysik
Institut für Extraterrestrische Physik
D-8046 Garching
Federal Republic of Germany

G. J. Stacey
Department of Physics
Birge Hall
University of California
Berkeley, CA 94720

J. B. Lugten
Institute for Astronomy
2680 Woodlawn Drive
Honolulu, Hawaii 96822

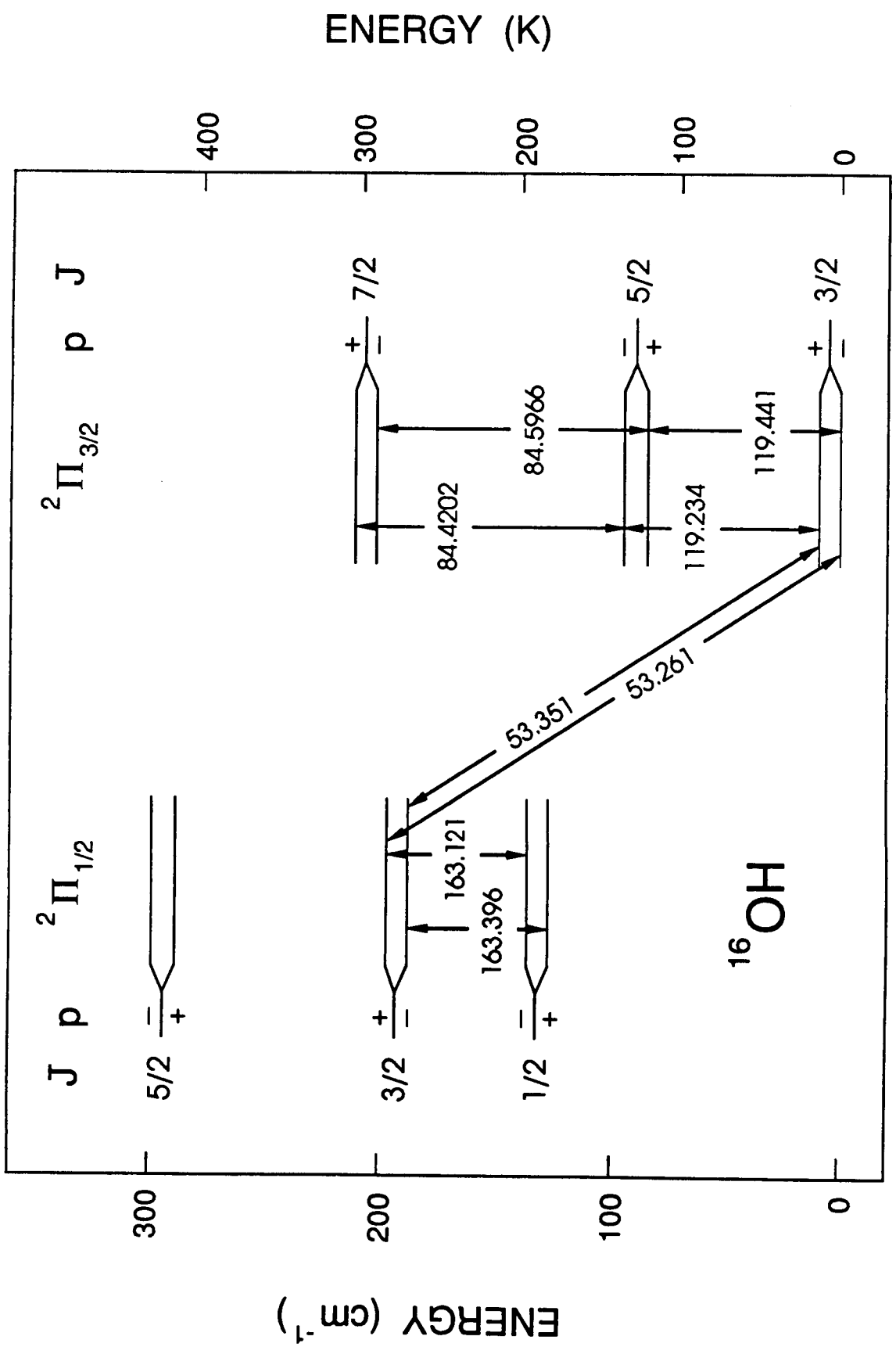
ENERGY (K)
400
300
200
100
0
$^2\Pi_{3/2}$
p
J
+
−
7/2
5/2
3/2
84.5966
119.441
84.4202
119.234
53.351
53.261
$^2\Pi_{1/2}$
J
p
5/2
3/2
1/2
163.121
163.396
^{16}OH
300
200
100
0
ENERGY (cm^{-1})

Figure 1

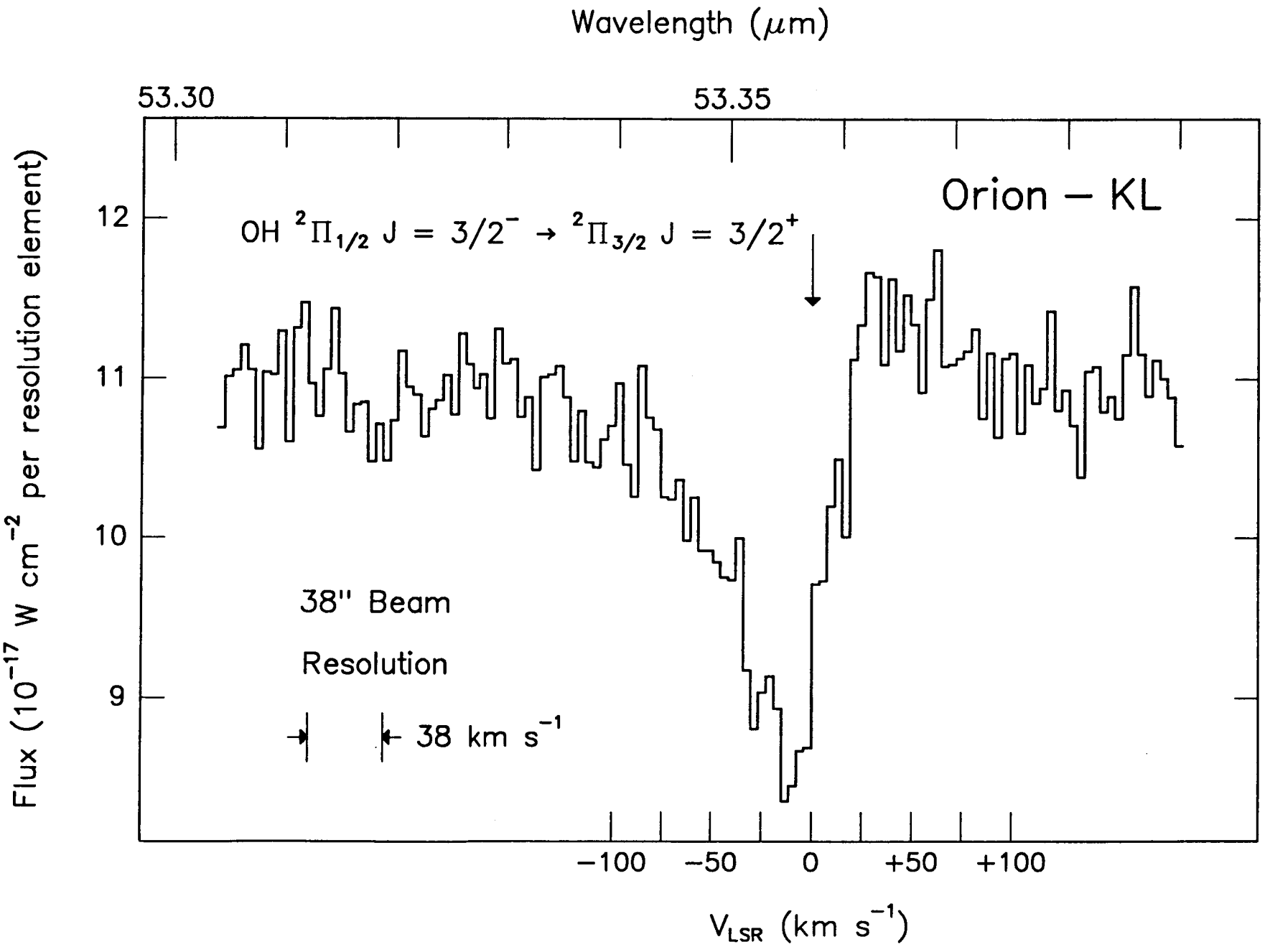
Wavelength (μm)
53.30
53.35
Orion – KL
OH $^2\Pi_{1/2}$ J = 3/2$^-$ → $^2\Pi_{3/2}$ J = 3/2$^+$
12
11
10
9
38" Beam
Resolution
38 km s^{-1}
Flux (10^{-17} W cm^{-2} per resolution element)
−100
−50
0
+50
+100
V_{LSR} (km s^{-1})

Figure 2

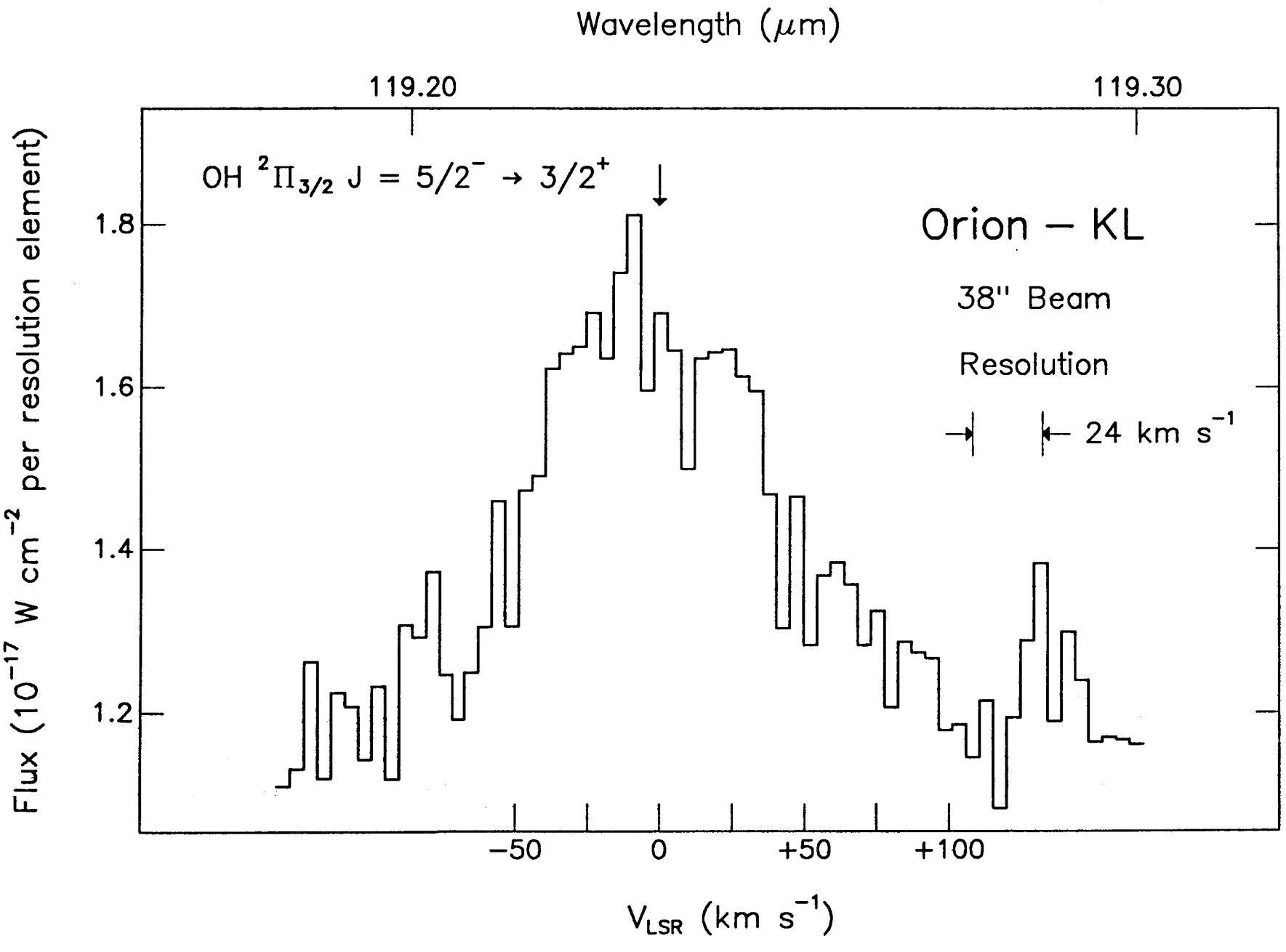
Wavelength (μm)
119.20
119.30
OH $^2\Pi_{3/2}$ J = 5/2$^-$ → 3/2$^+$
Orion – KL
38" Beam
Resolution
24 km s^{-1}
1.8
1.6
1.4
1.2
Flux (10^{-17} W cm^{-2} per resolution element)
−50
0
+50
+100
V_{LSR} (km s^{-1})

Figure 3

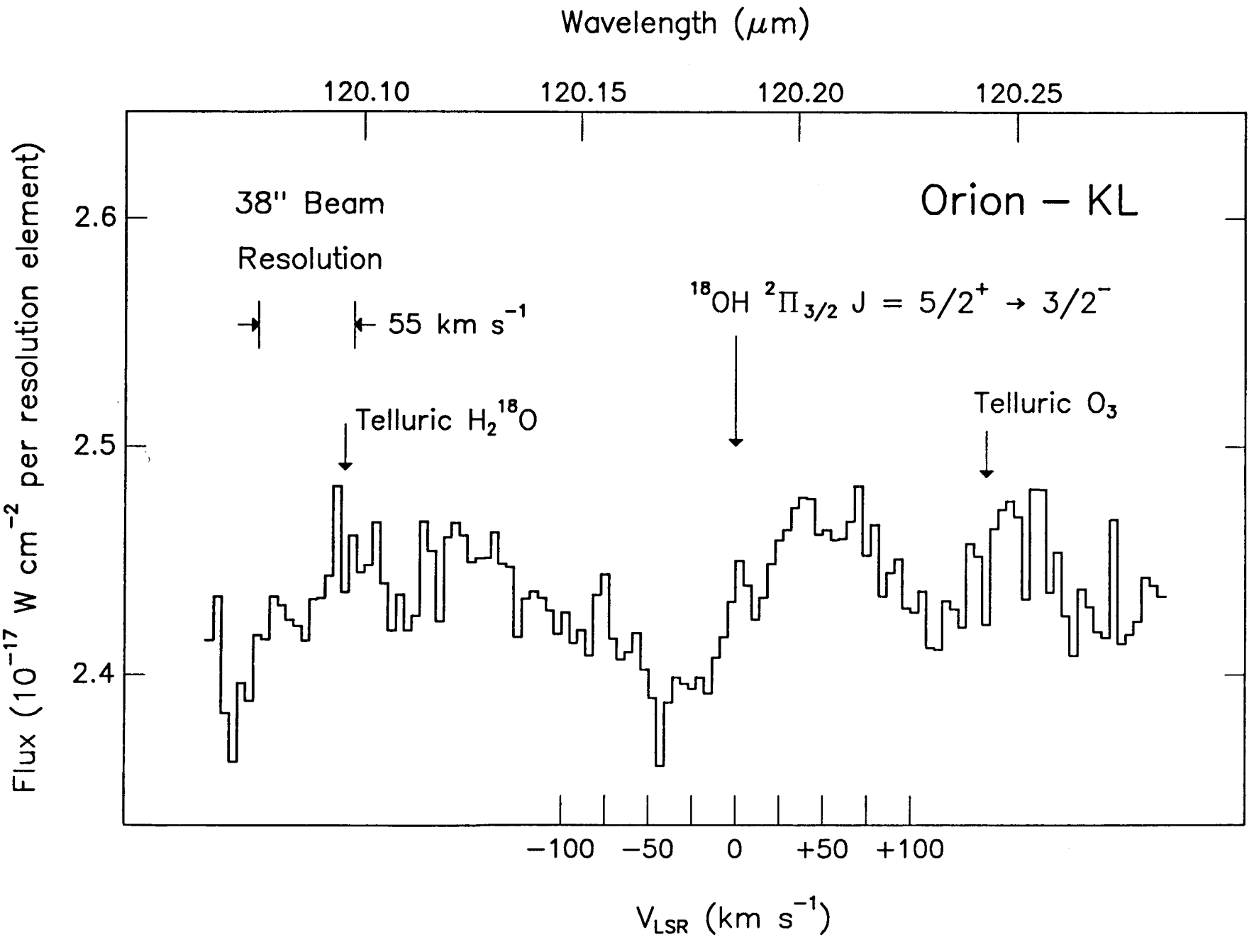
Wavelength (μm)
120.10
120.15
120.20
120.25
38" Beam
Resolution
55 km s^{-1}
Orion – KL
^{18}OH $^{2}\Pi_{3/2}$ J = 5/2^{+} → 3/2^{-}
Telluric $H_2{}^{18}O$
Telluric O_3
2.6
2.5
2.4
Flux (10^{-17} W cm^{-2} per resolution element)
−100
−50
0
+50
+100
V_{LSR} (km s^{-1})

Figure 4

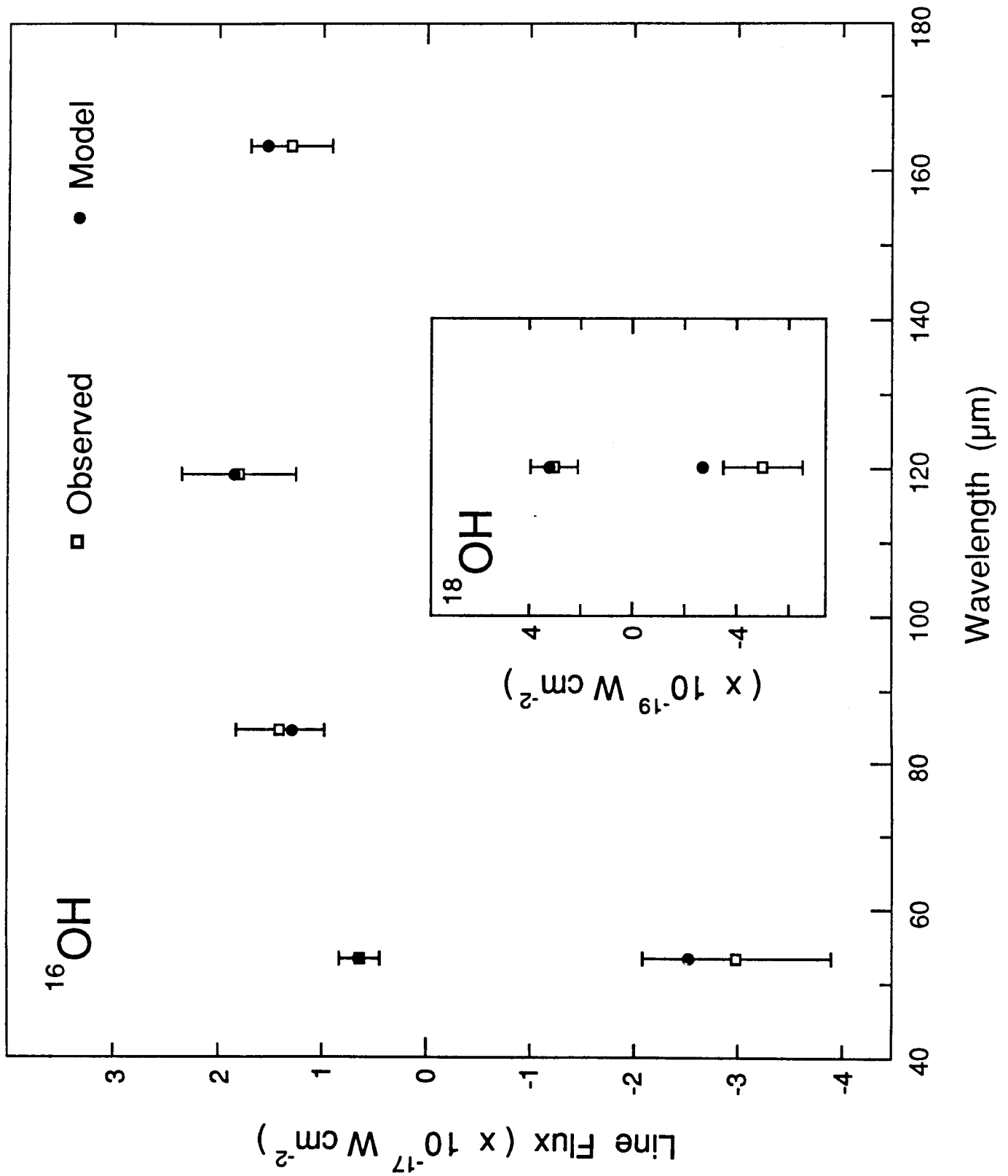
^{16}OH
Observed
Model
^{18}OH
Line Flux (x 10^{-17} W cm^{-2})
(x 10^{-19} W cm^{-2})
Wavelength (μm)
3
2
1
0
-1
-2
-3
-4
4
0
-4
40
60
80
100
120
140
160
180

Figure 5

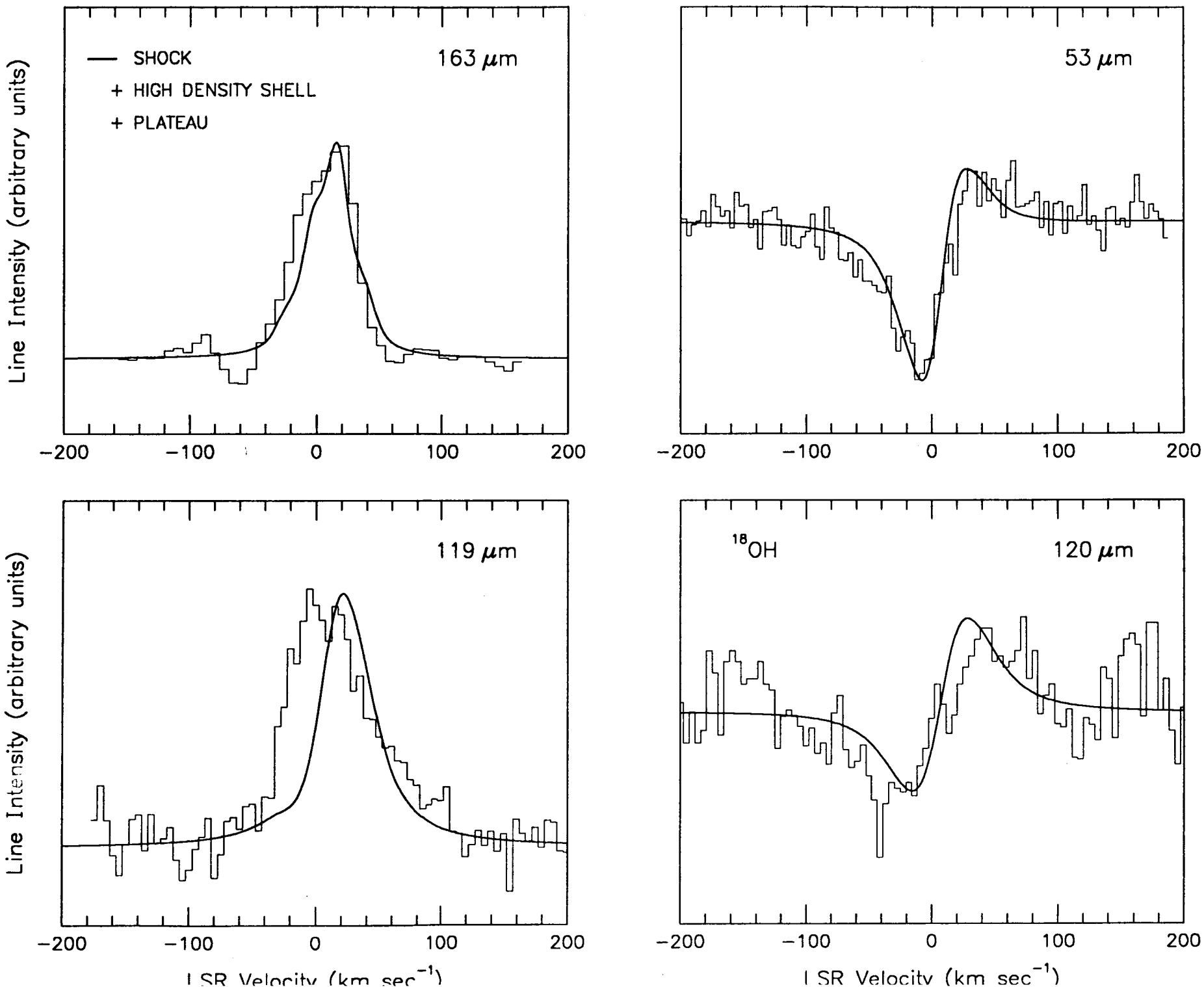
SHOCK
+ HIGH DENSITY SHELL
+ PLATEAU
163 μm
53 μm
119 μm
18OH
120 μm
Line Intensity (arbitrary units)
Line Intensity (arbitrary units)
−200
−100
0
100
200
−200
−100
0
100
200
−200
−100
0
100
200
−200
−100
0
100
200
LSR Velocity (km sec−1)
LSR Velocity (km sec−1)

Figure 6

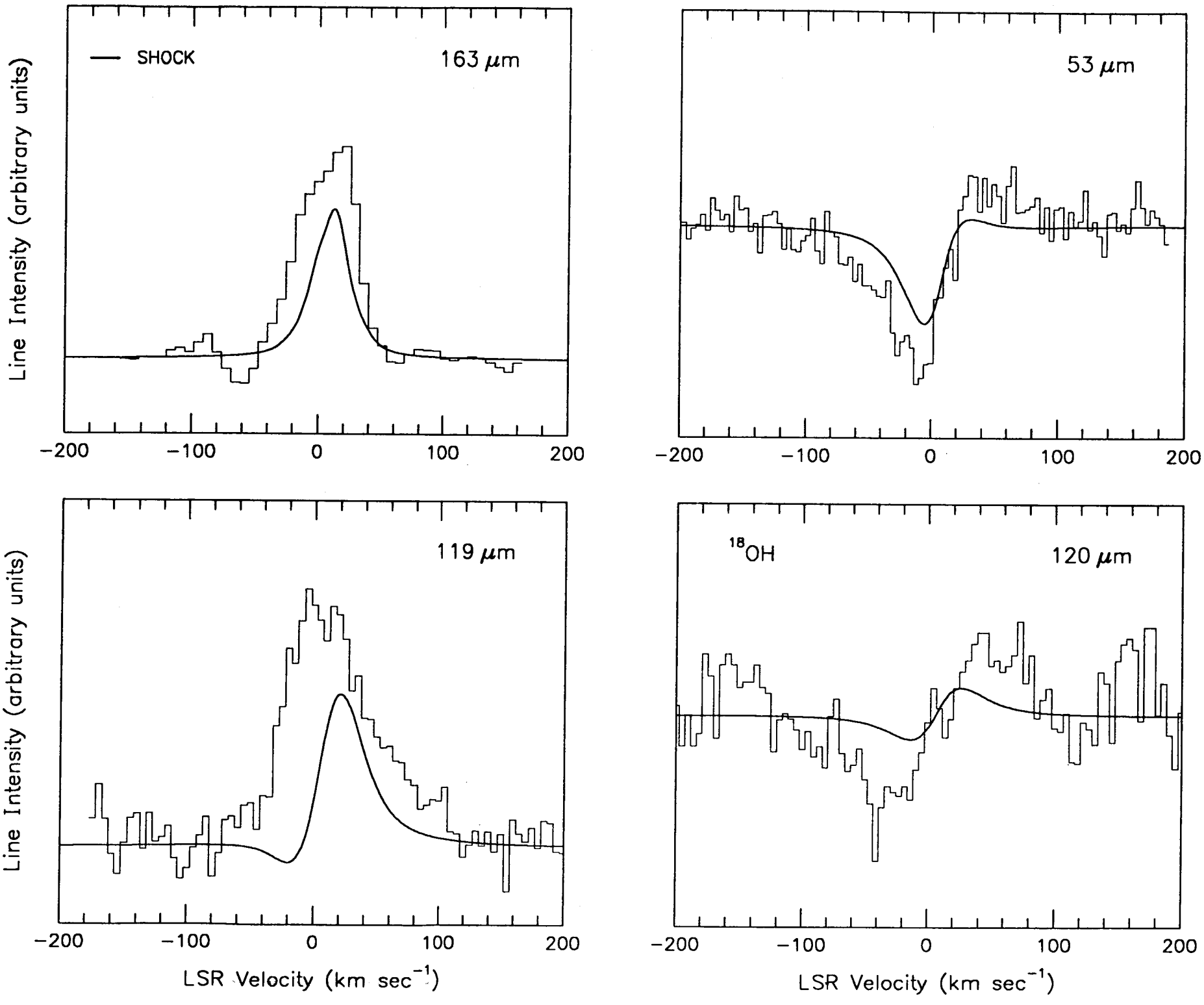
SHOCK
163 μm
53 μm
119 μm
^{18}OH
120 μm
Line Intensity (arbitrary units)
Line Intensity (arbitrary units)
−200
−100
0
100
200
LSR Velocity (km sec^{-1})
LSR Velocity (km sec^{-1})

Figure 7

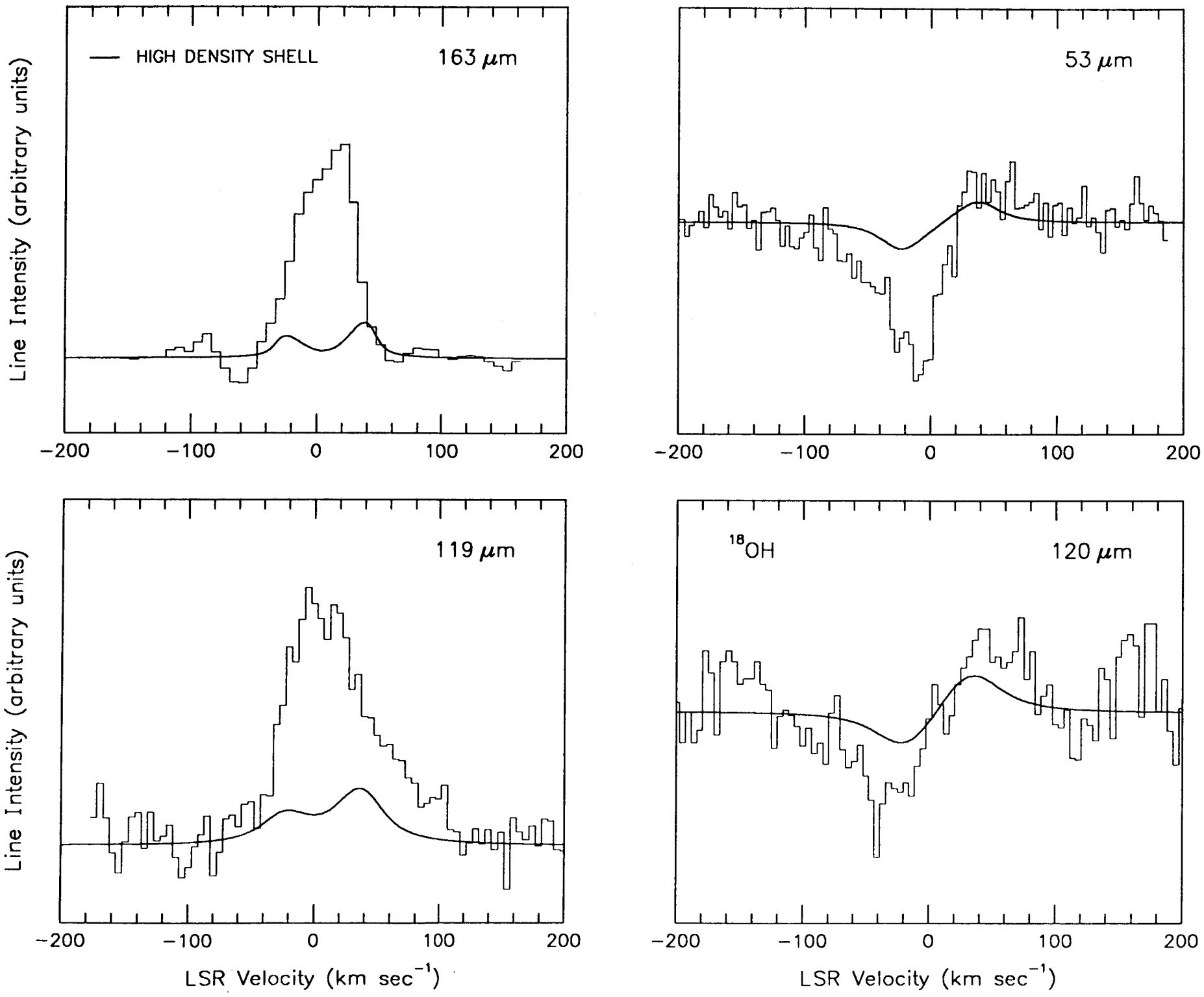
HIGH DENSITY SHELL
163 μm
53 μm
119 μm
^{18}OH
120 μm
Line Intensity (arbitrary units)
Line Intensity (arbitrary units)
−200
−100
0
100
200
LSR Velocity (km sec^{-1})
LSR Velocity (km sec^{-1})

Figure 8

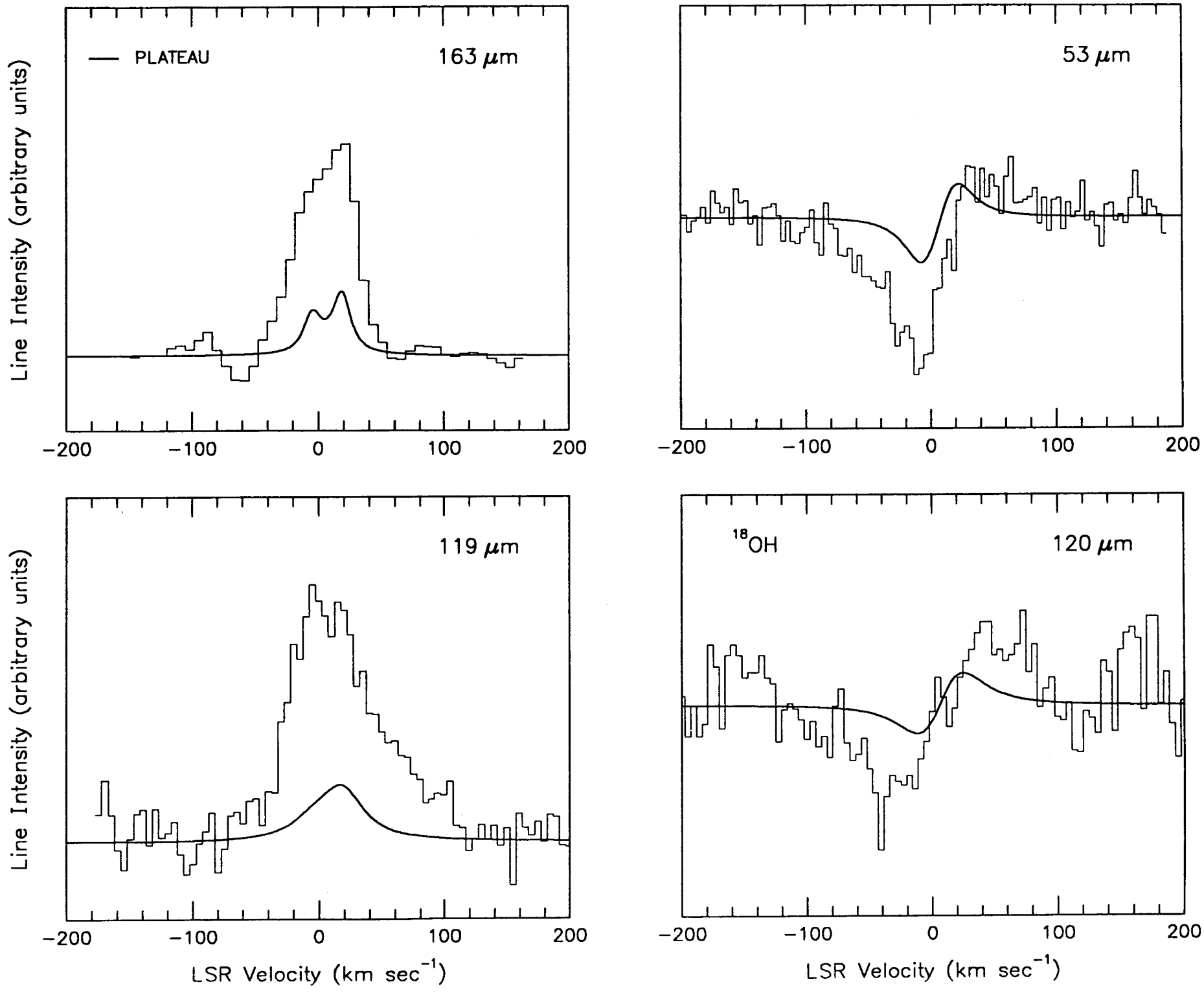
PLATEAU
163 μm
53 μm
119 μm
^{18}OH
120 μm
Line Intensity (arbitrary units)
Line Intensity (arbitrary units)
−200
−100
0
100
200
LSR Velocity (km sec^{-1})
LSR Velocity (km sec^{-1})

Figure 9